

# Ultrafast transient reflectivity measurements of optimally doped $\text{Bi}_{2+x}\text{Sr}_{2-x}\text{CaCu}_2\text{O}_{8+\delta}$ with disorder

Y. Toda  and S. Tsuchiya*Department of Applied Physics, Hokkaido University, Sapporo 060-8628, Japan*

M. Oda, T. Kurosawa, and S. Katsumata

*Department of Physics, Hokkaido University, Sapporo 060-0810, Japan*M. Naseska, T. Mertelj , and D. Mihailovic*Complex Matter Dept., Jozef Stefan Institute, Jamova 39, Ljubljana, SI-1000, Slovenia*

(Received 8 June 2021; revised 5 August 2021; accepted 26 August 2021; published 7 September 2021)

The effect of disorder in high- $T_c$  superconductors is investigated from the viewpoint of photoinduced quasiparticle (QP) dynamics, obtained through time-resolved pump-probe spectroscopy. We perform the measurements on an optimally doped (OPD)  $\text{Bi}_{2+x}\text{Sr}_{2-x}\text{CaCu}_2\text{O}_{8+\delta}$  (Bi2212) with an out-of-plane disorder induced by Bi-Sr substitution ( $x$ ), which is present in standard Bi2212 but is not usually controlled. Based on the systematic change of the disorder with controlled  $x$ , we identify the changes in the dynamics of QP relaxation and gap formation in superconducting (SC) and pseudogap (PG) states. The onset temperature  $T^*$  of the PG response increases with an increase in  $x$ , which is more significant than the slight decrease in  $T_c$ . These properties are equivalently reflected in the destruction fluences of the SC and PG states. Bi-Sr substitution also accelerates relaxation times for SC and PG QPs, which can be due to the increased phonon scattering probability caused by the disorder. In contrast, the SC gap recovery observed in the strongly excited condition shows an identical fluence dependence for various  $x$ , implying that the disorder does not significantly contribute to coherent gap formation.

DOI: [10.1103/PhysRevB.104.094507](https://doi.org/10.1103/PhysRevB.104.094507)

## I. INTRODUCTION

The pseudogap (PG) observed in hole-doped high- $T_c$  superconducting cuprates is a unique electronic state that appears in the temperature region above  $T_c$  and has been intensively studied as a key in elucidating the mechanism of high- $T_c$  superconductivity [1]. The PG usually develops in the low-hole-doping region with strong antiferromagnetic correlations and exhibits properties such as charge order, stripe order, and nematic order [2–15]. Direct observation of the checkerboard charge order in real space has been demonstrated through scanning tunneling microscopy and spectroscopy (STM/STS) [2–7]. The characteristic structure of the PG has been observed in momentum space through angle-resolved photoemission spectroscopy (ARPES), which shows that above  $T_c$ , a gap opens at the Fermi surface near the edge of the Brillouin zone, leaving a gapless Fermi arc around the Brillouin zone diagonal [16–19]. In contrast, in the temperature region below  $T_c$ , the PG shares the Fermi surface with the  $d$ -wave superconducting (SC) gap appearing in the node region, which is called the Fermi surface dichotomy [20,21]. Here, the ratio of the SC region to the PG in the momentum space depends on the doping level, and as the hole concentration decreases from the optimally doped (OPD) SC to underdoped (UD) SC, the PG region expands while the SC region shrinks, suggesting a competitive relationship between them.

In Bi-based cuprates, the PG can also be manipulated by controlling an out-of-plane disorder, which is caused by a substitution at Sr in the Sr-O plane by other atoms [22,23]. For example, in  $\text{Bi}_2\text{Sr}_{2-x}\text{R}_x\text{CuO}_{6+\delta}$  (R-Bi2201), by the substitution of Sr with lanthanides (R) from La to Eu, the Fermi arc shrinks and the PG energy and its spatial inhomogeneity increase, as observed by ARPES and STM/STS, respectively [24–26]. The correlation between spatial inhomogeneities and the PG has also been observed through STM/STS experiments in Bi2212, wherein the PG energy gap is spatially inhomogeneous, unlike the spatially uniform SC gap [7,27,28].

In this study, we investigated the effect of disorders on the SC and PG states through ultrafast photoinduced dynamics in  $\text{Bi}_{2+x}\text{Sr}_{2-x}\text{CaCu}_2\text{O}_{8+\delta}$  (Bi2212) with varying Bi-Sr substitutions ( $x$ ). Photoexcited nonequilibrium QPs facilitate the investigation of the relaxation properties and formation dynamics of the SC gap and the PG as well as their relationship [29–37]. In Bi2212, in particular, there is a distinct difference in the transient optical response properties between the SC and PG, allowing us to separate and compare their features using time-resolved analysis and spectral decomposition [36,37]. The characteristics of the PG have been explained through QP dynamics, for example, the temperature-independent gap energy [38], the absence of a critical slowdown due to collective excitations [39], the

relaxation anomaly in the presence or absence of SC [40], and correlation with SC in recovery dynamics [36].

In this study, we introduce the disorder by the Bi-Sr substitution ( $x$ ), which is present even in standard Bi2212 samples but is not usually controlled. Based on the systematic changes in the out-of-plane disorder induced by carefully controlled  $x$ , the changes in the dynamics of the QP relaxation and gap formation in the SC and PG states due to quenched disorder were identified. Our observations show that the onset temperature  $T^*$  of the PG response increases with an increase in  $x$ , and the magnitude of the increase is more significant than a slight decrease in  $T_c$  as  $x$  increases. Under weakly excited conditions the pump fluence dependence of the recombination time of the SC QP becomes stronger as  $x$  increases. In contrast, the relaxation time of the PG QPs shows a fluence-independent value, whereas its temperature dependence becomes weaker as  $x$  increases. These results suggest that the efficiency of the QP relaxation increases with an increase in  $x$  for both the SC and PG states, which can be understood as an enhancement of the coupling between high-energy and low-energy phonons due to the increased scattering probability caused by the disorder. In contrast, the SC gap recovery dynamics observed after a quench shows identical fluence dependence for all  $x$ , indicating that spatial inhomogeneity promotes QP pairing recombination but is ineffective in the formation of the SC order.

## II. EXPERIMENTAL

Single crystals of OPD  $\text{Bi}_{2+x}\text{Sr}_{2-x}\text{CaCu}_2\text{O}_{8+\delta}$  with varying systematic variation of  $x$  ( $= 0.10, 0.15, 0.20, 0.25$ ) were grown by the traveling solvent floating zone method. Here the out-of-plane disorder is induced by the Bi-Sr substitution ( $x$ ) in the Sr-O plane, which changes the position of the apical oxygen and indirectly induces the disorder in the conducting Cu-O plane [22,23]. Each sample was optimized for optimal doping by controlling the excess oxygen content  $\delta$ , which was confirmed by the annealing dependence of  $T_c$ . The temperature at which the normal state magnetic susceptibility reaches its maximum value ( $T_{\text{MAX}}$ ) systematically increases with an increase in  $x$  of the sample, indicating a systematic enhancement of the antiferromagnetic correlation by the substitution [41–43]. We also prepared an underdoped (UD)  $\text{Bi}_{2.2}\text{Sr}_{1.8}\text{CaCu}_2\text{O}_{8+\delta}$  ( $T_c = 69$  K) for comparison. In this study, the composition of Bi2212 is described in terms of the values of crystal growth.

The transient reflectivity change  $\Delta R/R$  was measured using a two-color pump-probe setup, wherein a 120 fs probe [ $E_{\text{pr}} = 1.55$  eV ( $\lambda_{\text{pr}} = 800$  nm)] and pump [ $E_{\text{pu}} = 3.1$  eV ( $\lambda_{\text{pu}} = 400$  nm)] pulses with a repetition rate of 270 kHz were obtained from a cavity dumped Ti: sapphire oscillator and its second harmonic. The pump and probe beams were superimposed coaxially with a time delay and then focused onto the  $ab$  plane of the cleaved crystal by a lens ( $f = 17$  mm), where the beam widths (diameter) are estimated to be 28  $\mu\text{m}$  (pump) and 22  $\mu\text{m}$  (probe), respectively. We focused on the  $A_{1g}$  transient dynamics, which is weighted isotropic around the  $\Gamma$  point [38] by extracting the isotropic polarization component from seven responses detected by rotating the polarization angle of the

probe every 45 degrees. This procedure also improves the signal-to-noise ratio by accumulating signals.

## III. RESULTS

### A. Temperature dependence

Figure 1(a) shows the density plots of  $\Delta R/R$  in a series of OPD Bi2212 with different  $x$  values at the pump fluence  $\mathcal{F} = 2.2$   $\mu\text{J}/\text{cm}^2$  and displayed with respect to the delay time (horizontal axis) and temperature (vertical axis). The rightmost column shows the results for the UD Bi2212 for comparison. The dominant signal in the low-temperature region below  $T_c$ , which is commonly observed in Fig. 1(a), is attributed to the QP relaxation dynamics associated with the superconductivity. The onset temperature of this component (corresponding to  $T_c$ ) in each sample was almost identical or slightly lower with an increase in  $x$  of the sample. Figure 1(b) shows the  $\Delta R/R$  at the lowest temperature and just below  $T_c$ . We can see the relaxation dynamics of the SC QPs on the timescale of the order of picoseconds, reflecting the QP recombination across the SC gap.

In the temperature region above  $T_c$  in Fig. 1(a), the relaxation dynamics of PG QPs that have a different sign from the SC response are visible. Previous studies have shown that the PG state signal under weak excitation conditions is generally smaller than that of the SC QP relaxation [36,37]. To clarify the PG state response Fig. 1(c) shows the temperature dependence of  $\Delta R/R$  measured at a higher pump fluence  $\mathcal{F} = 46$   $\mu\text{J}/\text{cm}^2$ . As discussed below, this fluence corresponds to the strong excitation condition that saturates the SC response. Under these conditions, the metallic electron-phonon relaxation (EPR) also appears in  $\Delta R/R$  with the same sign as the SC response as shown in Fig. 1(c), where the subpicosecond transient corresponds to the EPR response, which is highly distinct above  $T \sim 150$  K. Because this component is almost independent of temperature and is isolated above  $T \sim 200$  K, we excluded it from the analysis by subtracting the transient reflectivity measured at  $T = 250$  K  $> T^*$  from the data in Fig. 1(c). The density plots of the transient signal after subtraction ( $\Delta R_{\text{subt}}/R$ ) are shown in Fig. 1(d). The PG response is clearly distinct and disappears at  $T^* \approx 150$ –230 K, depending on the disorder, and shows a shift of  $T^*$  toward higher temperatures with an increase in  $x$ , which is the opposite trend to  $T_c$ . The normalized PG state transients  $\Delta R_{\text{subt}}/\Delta R_{\text{subt}}^{\text{max}}$  at temperatures just above  $T_c$  and close to  $T^*$  are shown in Fig. 1(e), showing that the relaxation time is of the order of subpicoseconds in all samples. Here, the amplitudes are normalized to their maximum values  $\Delta R_{\text{subt}}^{\text{max}}/R$ . Again, it should be noted that the PG response has the sign opposite to that of the SC response in the full  $T$  range. The  $T_c$  estimated from Figs. 1(c) and 1(d) are identical to those in Fig. 1(a), indicating that the thermal heating due to the repetition of pulse excitation is negligible at least up to  $\mathcal{F} = 46$   $\mu\text{J}/\text{cm}^2$ .

### B. Fluence dependence

The fluence dependences of the SC ( $T = 20$  K) and PG ( $T = 100$  K) responses in a series of substituted OPD samples are summarized in Fig. 2, and the results of the UD sample are also shown for comparison. To selectively analyze

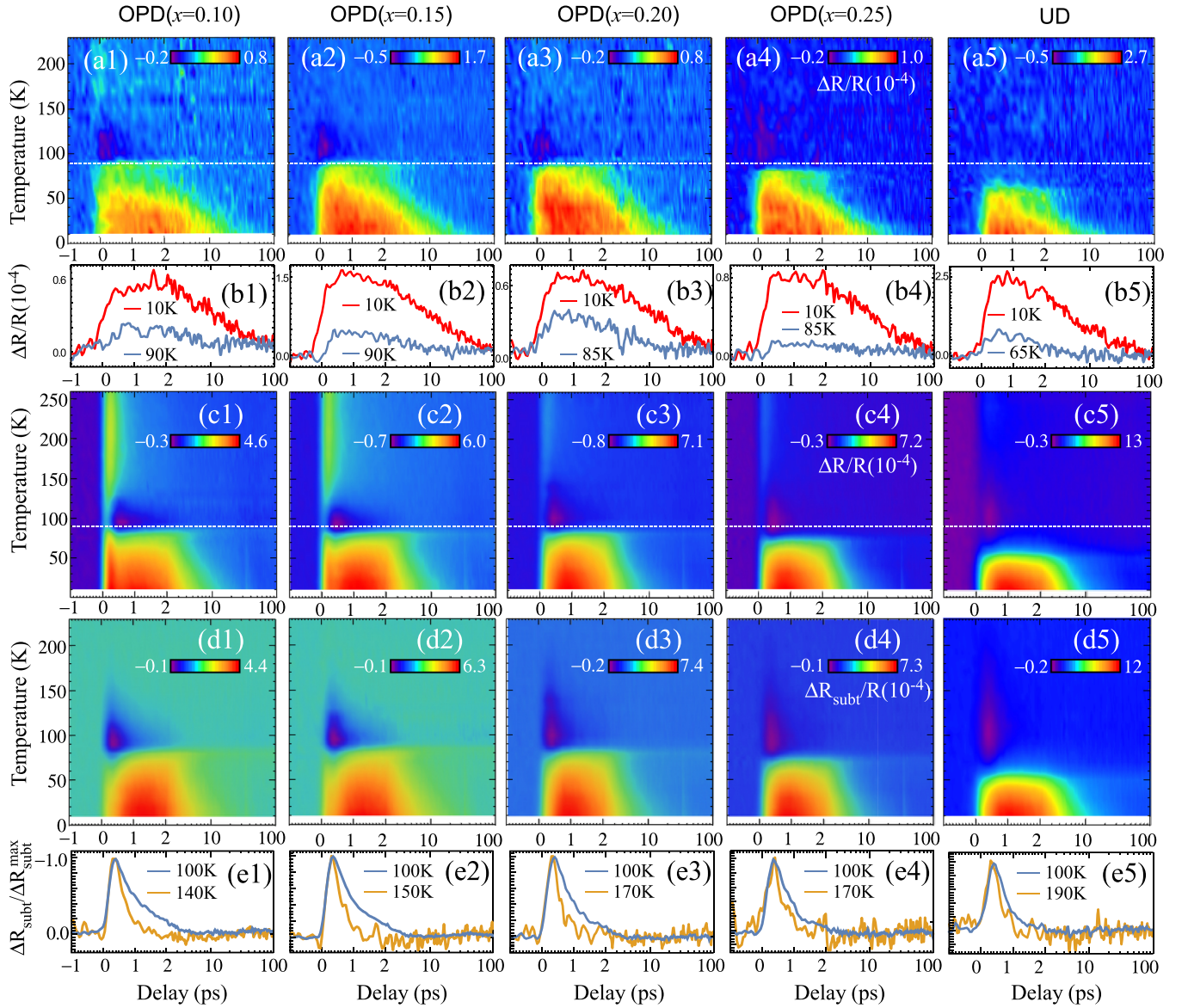


FIG. 1. (a) Density plots of  $\Delta R/R$  as functions of the delay time (horizontal axis) and temperature (vertical axis) for the OPD and UD Bi2212 samples, where the pump fluence is  $\mathcal{F} = 2.2 \mu\text{J}/\text{cm}^2$ , and  $x$  denotes the Bi-Sr substitution content. (b) Corresponding  $\Delta R/R$  transients at selected temperatures. (c) Same as (a), but obtained at  $\mathcal{F} = 46 \mu\text{J}/\text{cm}^2$ . The dashed lines in (a) and (c) indicate  $T = 90 \text{ K}$  for comparison purposes. (d) Density plots of  $\Delta R_{\text{subt}}/R$  obtained by subtracting the transients at  $T = 250 \text{ K}$  from  $\Delta R$  to remove the temperature-independent EPR response. (e) Corresponding  $\Delta R_{\text{subt}}/R$  transients at selected temperatures, where the sign of the vertical axis is reversed. The amplitudes are normalized to their maximum values  $\Delta R_{\text{subt}}^{\text{max}}/R$ .

the individual SC and PG components the PG and EPR responses included in the SC-dominated  $\Delta R/R$  below  $T_c$  and the EPR response included in the PG-dominated  $\Delta R/R$  above  $T_c$  and below  $T^*$  were removed using the subtraction technique [ $\Delta R_{\text{SC}} = \Delta R (T = 20 \text{ K}) - \Delta R (100 \text{ K})$  and  $\Delta R_{\text{PG}} = \Delta R (200 \text{ K}) - \Delta R (100 \text{ K})$ , respectively]. Here, we assume that the temperature dependences of the EPR and PG transients are sufficiently small in the relevant temperature regions. The  $\Delta R_{\text{SC,PG}}/R$  obtained based on the subtraction analyses at selected fluences are shown in Figs. 2(a) and 2(b), respectively. In each data, we see the individual dynamics of the SC and PG responses, confirming that the subtraction works well.

In Fig. 2(c), we plot the absolute amplitudes of the SC ( $A_{\text{SC}}$ , solid circles) and PG ( $A_{\text{PG}}$ , open squares) dynamics

with respect to the pump fluence. The  $A_{\text{SC}}$  and  $A_{\text{PG}}$ , respectively, show distinct saturation characteristics depending on the sample. A similar saturation has been observed in various electronic systems, including superconductors, corresponding to the destruction of the SC and PG states [44,45]. In Fig. 2(c), we plot  $A_{\text{SC}}$  and  $A_{\text{PG}}$  normalized to their saturation values together with the fits to the data (solid and dashed lines for  $A_{\text{SC}}$  and  $A_{\text{PG}}$ , respectively) using the analytical model for the finite-penetration-depth excitation [44]. In the model, we assume that the linearity of  $A$  is maintained until the SC/PG state is destroyed, and we define  $\mathcal{F}_{\text{th}}^{\text{SC}}$  ( $\mathcal{F}_{\text{th}}^{\text{PG}}$ ) as the threshold fluence required to destroy the SC (PG) state. We present the saturation thresholds  $\mathcal{F}_{\text{th}}^{\text{SC}}$  and  $\mathcal{F}_{\text{th}}^{\text{PG}}$  obtained from the model fits in each figure. As the Bi-Sr substitution increases,

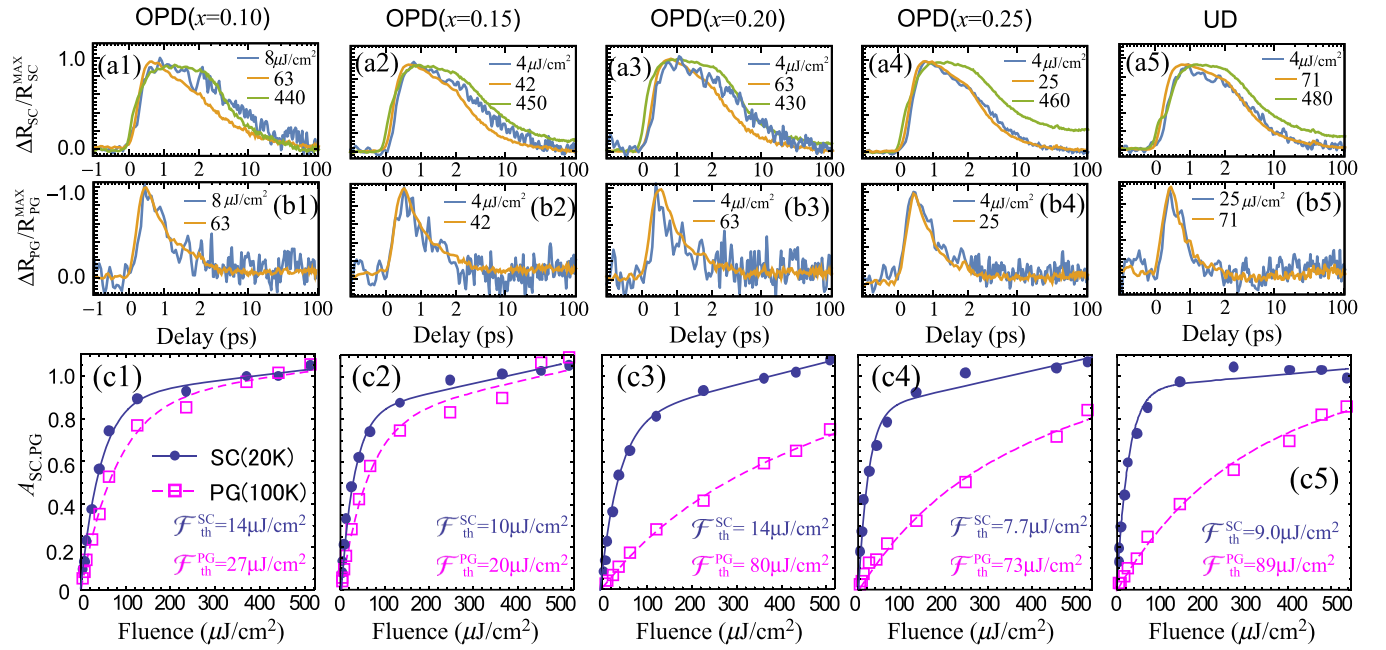


FIG. 2. The normalized transients of (a) SC and (b) PG responses at selected fluences, where individual SC and PG components were selected by  $\Delta R_{SC} = \Delta R (T = 20 \text{ K}) - \Delta R (100 \text{ K})$  and  $\Delta R_{PG} = \Delta R (200 \text{ K}) - \Delta R (100 \text{ K})$ , respectively. (c) Pump fluence dependence of the absolute amplitudes of the SC ( $A_{SC}$ , solid circles) and PG ( $A_{PG}$ , open squares) components, normalized to their saturation values, for OPDs with various  $x$  and UD Bi2212. The required threshold fluences to destroy the SC ( $\mathcal{F}_{th}^{SC}$ ) and PG ( $\mathcal{F}_{th}^{PG}$ ) states are also shown in each figure.

$\mathcal{F}_{th}^{SC}$  shows a slightly decreasing tendency (with large scatter), whereas  $\mathcal{F}_{th}^{PG}$  increases significantly, which is in agreement with the trends of  $T_c$  and  $T^*$  evaluated from the temperature dependencies in Fig. 1.

### C. Analysis

The temperature and fluence dependences of the amplitudes ( $A$ ) and relaxation times ( $\tau$ ) estimated by fitting a single exponential decay function to the transient reflectivity in Figs. 1 and 2 are summarized in Fig. 3. Figures 3(a) and 3(b) show the temperature dependences of the SC ( $A_{SC}$ ) and PG ( $A_{PG}$ ) amplitudes, respectively. Here, the amplitudes are normalized to the maximum value (the amplitude at the lowest temperature) to compare a series of samples with ease.  $A_{SC}$  was derived from the data in Fig. 1(a). Here, as shown in Fig. 2(c),  $\mathcal{F} = 2.2 \mu\text{J}/\text{cm}^2$  corresponds to the weak excitation condition with a linear fluence dependence of  $A_{SC}$ . Therefore, the photoexcited QPs and high-energy phonon densities can be assumed to be sufficiently lower than the equilibrium densities, and the temperature dependence of  $A_{SC}$  can be reproduced by the Kabanov model characterized by a perturbative high-energy phonon density distribution [46]. In Fig. 3(a), the results of the model fit the data with  $x = 0.10$  and 0.25 are shown as solid and dashed lines, respectively. Based on the gap function assuming the BCS temperature dependence,  $T_c$  is estimated to be 92, 92, 89, and 85 K for the samples with  $x = 0.10, 0.15, 0.20,$  and  $0.25$ , respectively. These values are consistent with those obtained from the magnetic susceptibility ( $T_c = 91, 88, 87,$  and  $83 \text{ K} \pm 1 \text{ K}$ , respectively).

The temperature dependence of  $A_{PG}$  [Fig. 3(b)], was derived from the data in Fig. 1(d). The gradual temperature

dependence of  $A_{PG}$  is approximated by the Kabanov model using a temperature-independent gap  $\Delta_{PG}^0$  [46]

$$A_{PG}(T) \propto \left[ 1 + A_1 \exp\left(-\frac{\Delta_{PG}^0}{k_B T}\right) \right]^{-1}, \quad (1)$$

where  $A_1$  is the ratio of the number of phonon degrees of freedom to the number of involved electronic states. The best-fit curves are shown by the solid ( $x = 0.10$ ) and dashed ( $x = 0.25$ ) lines in Fig. 3(b). The onset temperature of the PG component, i.e.,  $T^*$ , at which the value of the best-fit curve is equivalent to the background noise level (1/10 of the normalized amplitude  $A$ ), shifts to higher temperatures of  $\sim 167, 172, 200,$  and  $201 \text{ K}$  with an increase in  $x = 0.10\text{--}0.25$ , confirming the enhancement of the PG associated with the out-of-plane disorder. In contrast,  $\Delta_{PG}^0$  obtained from the fit of Eq. (1) shows a similar value (approximately 100 meV) for all the samples, as summarized in Fig. 3(c), together with the corresponding  $A_1$  values.  $A_1$  monotonically decreases with an increase in  $x$ ; however the magnitude is exceedingly high (higher than the typical value of around  $10^2$  [36,38]). Note that even when  $A_1$  has a huge error,  $\Delta_{PG}^0$  is not significantly affected, as indicated by the small error bars in  $\Delta_{PG}^0$ . The extremely high value of  $A_1$  is at least partially an artifact of the subtraction procedure. While  $\Delta_{PG}^0$  is set by the characteristic temperature of the  $A_{PG}(T)$  drop  $A_1$  is mostly set by the high- $T$  tail magnitude that is artificially removed by the subtraction procedure. Indeed,  $A_1$  approaches the typical value as  $x$  of the sample increases, and the contribution of the EPR becomes small as shown in Fig. 1(c). Moreover, the high- $T$  tail is additionally suppressed [beyond the scope of the Kabanov model in Eq. (1)] by the disappearance of the PG state above  $T^*$ . The increase in  $T^*$  with increasing  $x$  despite the  $x$  independent

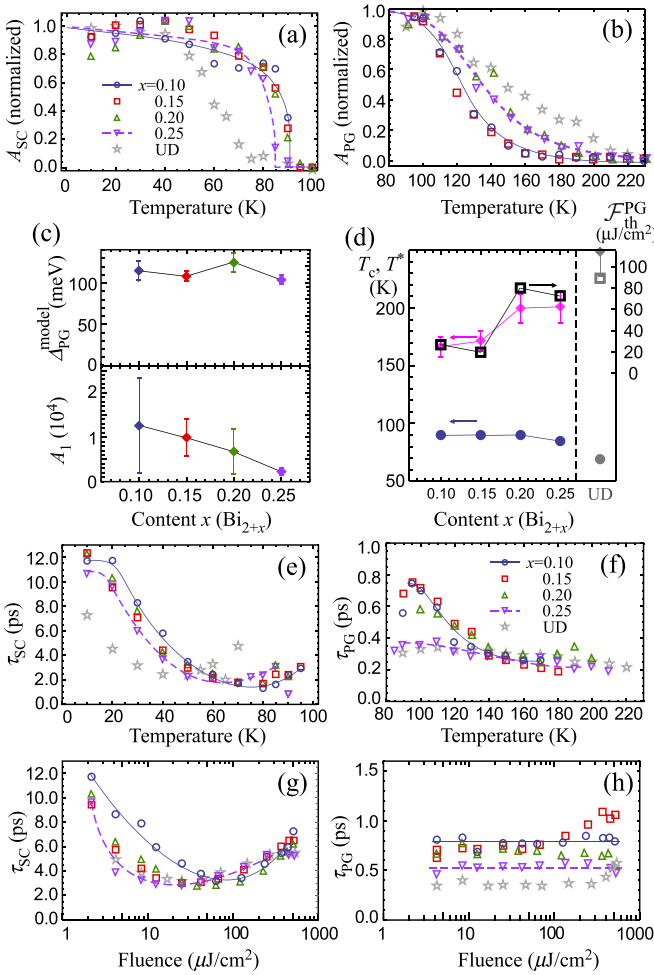


FIG. 3. The temperature dependences of (a) and (b) normalized amplitudes and (e) and (f) decay times for OPD with various  $x$  and UD Bi2212, where the data of (left) SC ( $\mathcal{F} = 2.2 \mu\text{J}/\text{cm}^2$ ) and (right) PG ( $\mathcal{F} = 46 \mu\text{J}/\text{cm}^2$ ) are obtained from the fits of the exponential decay function to the data in Figs. 1(a) and 1(d), respectively. (c) Summary of  $\Delta_{\text{PG}}^0$  (top) and  $A_1$  (bottom) obtained from the fit of Eq. (1) for data in (b). (d) Plots of  $T_c$  and  $T^*$  for a series of samples evaluated from (a) and (b), respectively, together with  $\mathcal{F}_{\text{th}}^{\text{PG}}$  from Fig. 2(c). Pump fluence dependence of decay times for (g) SC ( $T = 20 \text{ K}$ ) and (h) PG ( $T = 100 \text{ K}$ ) components. Theoretical fits using Kabanov models [46] to the data for  $x = 0.10$  (solid line) and  $0.25$  (dashed line) are shown in (a) and (b). The lines in (e), (f), and (g) are guides for the eye. The horizontal lines in (h) are the average values for  $x = 0.10$  and  $0.25$ .

$\Delta_{\text{PG}}^0$  suggests that  $T^*$  [upper graph of Fig. 3(c)] also depends on the dynamical effects that are affected by the disorder.

Figure 3(d) shows  $T_c$  (solid circles) and  $T^*$  (solid diamonds) as a function of substitution  $x$  along with  $\mathcal{F}_{\text{th}}^{\text{PG}}$  (open squares). Because the photodestruction of the gap is indirect in both SC and PG systems, only a part of the energy reflected in  $\mathcal{F}_{\text{th}}^{\text{SC,PG}}$  is used to destroy the gap state, and most of the energy is consumed by low-energy phonon excitations given by a monotonic function of the gap size. This results in a linear relationship between  $\mathcal{F}_{\text{th}}^{\text{PG}}$  and the PG energy, which has already been demonstrated by the doping level dependence of

$\mathcal{F}_{\text{th}}^{\text{PG}}$  in Bi2212 [39]. In Fig. 3(d), we can see a similar relationship for a series of OPD samples with various disorders.

The temperature dependence of the relaxation times of the SC [ $\tau_{\text{SC}}$  derived from Fig. 1(a) at  $\mathcal{F} = 2.2 \mu\text{J}/\text{cm}^2$ ] and PG [ $\tau_{\text{PG}}$  derived from Fig. 1(d) at  $\mathcal{F} = 46 \mu\text{J}/\text{cm}^2$ ] dynamics are shown in Figs. 3(e) and 3(f), respectively. The  $\tau_{\text{SC}}$  in the weakly excited condition reflects the relaxation from the state in which the photoexcited QPs and high-energy phonons had already reached quasiequilibrium. Here, because the recombination of SC QPs is a second-order process that reflects a pair formation, the relaxation rate  $\Gamma_{\text{SC}} (= \tau_{\text{SC}}^{-1})$  is proportional to the total QP density given by the sum of the photoexcited ( $n_{\text{ph}}$ ) and thermally excited ( $n_{\text{T}}$ ) QPs;

$$\Gamma_{\text{SC}} = 2(n_{\text{ph}} + n_{\text{T}})\tilde{\gamma}_{\text{SC}}, \quad (2)$$

where  $\tilde{\gamma}_{\text{SC}}$  is the effective energy relaxation rate of high-energy phonons [47,48]. As a result, at a constant pump fluence at temperatures well below  $T_c$ ,  $\Gamma_{\text{SC}}$  becomes higher, i.e.,  $\tau_{\text{SC}}$  becomes shorter as the temperature increases. In contrast, as the temperature approaches  $T_c$   $\tau_{\text{SC}}$  shows an upturn reflecting the critical slowing down with the closing of the SC gap. In Fig. 3(e), the temperature dependence of  $\tau_{\text{SC}}$  for all samples corresponds well with the above equation, and the slight decrease in  $\tau_{\text{SC}}$  with  $x$  at low temperature is consistent with the slight decrease in  $T_c$  with  $x$ , which increases  $n_{\text{T}}$  and  $\tilde{\gamma}_{\text{SC}}$  in Eq. (2).

In contrast to the SC relaxation,  $\tau_{\text{PG}}$  decreases monotonically with an increase in temperature [Fig. 3(f)]. As shown in Fig. 3(b), the temperature dependence of the PG QP indicates the relaxation across the PG with temperature-independent energy and is associated with the localized PG nature [39] with no long-range order. In Fig. 3(f), the temperature dependence of  $\tau_{\text{PG}}$  becomes weaker as  $x$  increases.  $\tau_{\text{PG}}$  of the samples with  $x = 0.10$  decreases from 0.8 ps to 0.3 ps indicating an increase in the scattering probability with an increase in temperature. In contrast, for the  $x = 0.25$  sample,  $\tau_{\text{PG}}$  is already as fast as 0.3 ps at  $T = 100 \text{ K}$  and remains almost unchanged in the temperature range up to near  $T^*$ . These can also be seen directly from the data in Figs. 1(c) and 1(d). It should be noted that  $\mathcal{F} = 46 \mu\text{J}/\text{cm}^2$  used to measure the temperature dependence of  $\tau_{\text{PG}}$  exceeds  $\mathcal{F}_{\text{th}}^{\text{PG}}$  of samples with smaller  $x$  (0.10 and 0.15). However, as shown in Fig. 3(h), the fluence dependence of  $\tau_{\text{PG}}$  is small and hardly changes around  $\mathcal{F}_{\text{th}}^{\text{PG}}$ . Therefore, the temperature and sample dependence of  $\tau_{\text{PG}}$  can be considered as an intrinsic property independent of  $\mathcal{F}$ .

The fluence dependence of  $\tau_{\text{SC}}$  ( $T = 20 \text{ K}$ ) and  $\tau_{\text{PG}}$  (100 K) are shown in Figs. 3(g) and 3(h), respectively. Here, the decay time  $\tau$  is plotted on the log scale of the fluence to emphasize the changes around the saturation threshold ( $\mathcal{F}_{\text{th}}$ ). In each sample,  $\tau_{\text{SC}}$  shows a parabolic dependence on the fluence [Fig. 3(g)], which can be explained by the combination of two types of dynamics: the QP relaxation across the constant SC gap under weak excitation conditions and the SC gap recovery dynamics upon quenching, under strong excitation conditions. As mentioned above, the relaxation rate of the SC QPs under weakly excited conditions is given by Eq. (2), and the increase of photoexcited QPs ( $n_{\text{ph}}$ ) with an increase in fluence leads to a decrease of  $\tau_{\text{SC}}$ . Here, the decrease rate of  $\tau_{\text{SC}}$

with fluence shows a systematic variation with the increase in  $x$ , which will be discussed in the Discussion section. A small decrease in  $\tau_{\text{SC}}$  [Fig. 3(e)] was observed, associated with an increase in  $x$  at the lowest fluence, which can be understood as a decrease in the thermally excited QP density ( $n_{\text{T}}$ ) and the effective relaxation rate of high-energy phonons ( $\tilde{\gamma}_{\text{SC}}$ ) owing to a slight decrease of the SC gap energy with the increase in  $x$ .

In contrast, the QP dynamics under strongly excited conditions above  $\mathcal{F}_{\text{th}}^{\text{SC}}$  correspond to the recovery of the SC order parameter after an optical quench [40], reflecting the coherent gap formation; thus  $\tau_{\text{SC}}$  effectively increases as the excitation fluence increases. The fluence dependence of the order-parameter dynamics in Bi2212 has been precisely investigated in three-pulse coherent quench experiments and is in good agreement with the current results.

In contrast,  $\tau_{\text{PG}}$  is nearly independent of the fluence [Fig. 3(h)]. In the figure, the horizontal lines represent the average values of the  $\tau_{\text{PG}}$  measured for the  $x = 0.10$  and  $x = 0.25$  samples, and we can see that  $\tau_{\text{PG}}$  in each sample is almost constant for all fluences. The different magnitudes of  $\tau_{\text{PG}}$  depending on the samples correspond to the different temperature dependences of  $\tau_{\text{PG}}$  for the samples shown in Fig. 3(f), where the results at  $T = 100$  K show a decrease in the  $\tau_{\text{PG}}$  with an increase in  $x$ . Furthermore, the saturation of  $A_{\text{PG}}$  [Fig. 2(c)] with the increase in  $\mathcal{F}$  does not influence  $\tau_{\text{PG}}$  in Fig. 3(h), i.e., the photoexcitation above  $\mathcal{F}_{\text{th}}^{\text{PG}}$  does not change the PG energy. A similar fluence independence of PG dynamics has already been reported for PG recovery dynamics [39] and was attributed to the localized nature of the PG. In this case, the saturation property of the PG dynamics can be attributed to the photoexcitation of all carriers from the localized state to the itinerant state. Thus, its energy does not change throughout the saturation condition.

#### IV. DISCUSSION

We discuss the SC and PG properties of OPD Bi2212, focusing on the changes in the QP dynamics due to the out-of-plane disorder. The most significant change with the increase in  $x$  is the enhancement of the PG, which can be seen in both the temperature and fluence dependences of  $A_{\text{PG}}$ . The PG temperature  $T^*$  increases by  $\sim 30$  K (from  $\sim 167$  to 201 K) with the increase in  $x$  from 0.10 to 0.25, whereas  $T_{\text{c}}$  decreases by  $\sim 7$  K (from 92 to 85 K) in Figs. 3(a) and 3(b). Similarly, the  $\mathcal{F}_{\text{th}}^{\text{PG}}$  of the samples with  $x = 0.20$  and 0.25 are approximately three to four times higher than that of the samples with  $x = 0.10$  and 0.15 and reaches a similar value as in the UD Bi2212 [Fig. 3(d)]. Similar trends were observed in R-Bi2201 (R=Eu, La) using ARPES and STM/STS, where the PG energy was significantly enhanced by increasing the disorder (La  $\rightarrow$  Eu) compared to the suppression of the SC gap, and the magnitude of the enhancement (suppression) of the PG (SC gap) is in good agreement with the underdoping of La-Bi2201 [24–26]. Note that in contrast to the Bi2201 case, the decrease in  $T_{\text{c}}$  by  $x$  in the OPD Bi2212 is smaller than the decrease in  $T_{\text{c}}$  in the UD sample, while the increase in  $T^*$  in the disordered OPD is comparable to that in the UD. The rather significant  $T^*$  dependence on the disorder indicates that the disorder mainly increases the PG energy, which may

provide an important clue for understanding the origin of the PG.

In Fig. 3(c), we mentioned that  $\Delta_{\text{PG}}^0$  from the Kabanov model fits [Eq. (1)] is independent of the disorder and thus does not correlate with  $T^*$  although the results include errors due to the subtraction of the data. Based on this idea,  $\Delta_{\text{PG}}^0$  can be regarded as a static property determined by doping. The disorder increases the pinning of the electronic inhomogeneity, and the fluctuations are suppressed at higher  $T$ , thus resulting in an increased  $T^*$ .

The contribution of the disorder to the PG can also be seen in the temperature dependence of  $\tau_{\text{PG}}$  [Fig. 3(f)], which varies with  $x$ . In Fig. 3(h),  $\tau_{\text{PG}}$  is independent of the excitation fluence, i.e., independent of the QP density and saturation conditions. Moreover, as shown in Fig. 3(b), the temperature dependence of  $A_{\text{PG}}$  indicates that  $\Delta_{\text{PG}}^0$  is independent of temperature. Based on these observations, the systematic change in the temperature dependence of  $\tau_{\text{PG}}$  with  $x$  in Fig. 3(f) is attributed to the changes in the interaction between the low-energy and high-energy phonons, which affects the bottleneck relaxation rate of the PG QPs. The spatial inhomogeneity introduced by the disorder reduces the symmetry and momentum limitations of the interaction between the phonons, as well as increases the scattering probability for the PG QPs. In Fig. 3(f), we also see that the temperature dependence of  $\tau_{\text{PG}}$  observed in the OPD sample with  $x = 0.25$  is almost identical to that of the UD sample, as is the case for  $\mathcal{F}_{\text{th}}^{\text{PG}}$ , suggesting that spatial inhomogeneity plays an important role in the enhancement of PG in the UD sample. This result corresponds well with the observations from the STM/STS of Bi2212, where the PG enhancement is correlated with spatial inhomogeneity [7,26,27].

The effect of the out-of-plane disorder on the SC QP dynamics is manifested in the fluence dependence of  $\tau_{\text{SC}}$ . In Fig. 3(g),  $\tau_{\text{SC}}$  under weakly excited conditions decreases with the pump fluence, and its slope (decrease rate) increases with  $x$ . Because the relaxation rate in the SC state ( $\Gamma_{\text{SC}}$ ) is given by Eq. (2), the increase in the photoexcited QP density ( $n_{\text{ph}}$ ) with an increase in fluence leads to a decrease in  $\tau_{\text{SC}}$ . Moreover, the thermally excited QP density ( $n_{\text{T}}$ ) decreases when the SC gap energy increases. In fact, at the minimum fluence, as shown in Fig. 3(g), we observe a systematic decrease in  $\tau_{\text{SC}}$  with  $x$ , which is consistent with the slight decrease of the SC gap energy in Fig. 3(a). However, because the SC gap is nearly constant with respect to the fluence under weakly excited conditions, the changes in the decreasing rate of  $\tau_{\text{SC}}$  with  $x$  in Fig. 3(g) cannot be explained by the decrease in the SC gap. From Eq. (2), we see that an increase in  $\tilde{\gamma}_{\text{SC}}$  can change the rate of decrease. The increase in the scattering probability due to disorder increases the effective relaxation rate of the hot phonons  $\tilde{\gamma}_{\text{SC}}$ , resulting in more efficient QP pair recombination. Namely, the disorder resulting from the substitution induces efficient relaxation for both PG and SC QPs at least under the weakly excited conditions.

In contrast, in the strongly excited region,  $\tau_{\text{SC}}$  converges to the same excitation fluence dependence for all samples, suggesting that the SC state recovery dynamics are not affected by the disorder. This is correlated with the absence of a significant suppression of  $T_{\text{c}}$  with increasing  $x$ , which

is smaller than the significant enhancement of  $T^*$  with an increase in  $x$ .

To complete the analysis, we consider  $\tau_{SC}$  in the crossover between weak and strong excitations. We see that the  $\tau_{SC}$  for each sample shows a minimum value at a fluence above the saturation threshold ( $\mathcal{F}_{th}^{SC} \approx 10\text{--}20 \mu\text{J}/\text{cm}^2$ ). This fluence is different for each sample but is determined by the similar value of  $\tau_{SC} \approx 3.0$  ps, which corresponds to the response time for the gap recovery [40]. In other words, the lower limit of  $\tau_{SC}$  is fixed by the order-parameter dynamics. It is important to note that the SC order parameter, which grows from a fluctuating background [40,49], is highly inhomogeneous in this intermediate  $F$  range. The cleanest  $x = 0.10$  sample shows a minimum of  $\tau_{SC}$  significantly above  $\mathcal{F}_{th}^{SC}$  than the  $x > 0.10$  samples, reflecting the possibility that the SC state is less completely suppressed well above  $\mathcal{F}_{th}^{SC}$  in the  $x = 0.10$  sample. While the (quasi)equilibrium SC appears quite robust with respect to the disorder the highly nonequilibrium fluctuating SC appears more fragile.

## V. CONCLUSION

In summary, we investigated the effect of the out-of-plane disorder on the SC and PG states through photoinduced QP dynamics in OPD Bi2212 with systematic Bi-Sr substitutions. The Bi-Sr substitution is present even in standard Bi2212 samples but is not usually controlled. In this study, we controlled this parameter and identified the changes in the dynamics of the QP relaxation and gap formation in the SC and PG states due to quenched disorder.

The transient response amplitude  $A_{PG}$  in the disordered sample reveals a significant enhancement of the PG compared to the suppression of the SC gap in both the temperature and saturation fluence characteristics, which is more noticeable compared to the results observed in the UD sample, whereas the PG of the disordered OPD is comparable to that of the UD sample, while the suppression of the SC gap of the disordered sample is smaller than that of the UD.

The relaxation time of the PG QPs  $\tau_{PG}$  is independent of the fluence for all samples, indicating the localized nature of the PG. This is also consistent with the temperature-independent gap observed in the temperature dependence of  $A_{PG}$ . In contrast, the temperature dependence of  $\tau_{PG}$  shows a systematic decrease with an increase in the disorder, indicating an increased effective relaxation for the PG QPs.

The efficiency of the QP relaxation also increases for the SC state in the disordered sample, which is mainly manifested in the fluence dependence of  $\tau_{SC}$  under weak excitation conditions, where a significant decrease in  $\tau_{SC}$  is observed with increasing fluence. In contrast,  $\tau_{SC}$  under strong excitation conditions reflects the SC gap recovery and shows a similar fluence dependence for all samples. To summarize, the disorder promotes QP pair recombination but does not contribute significantly to the coherent gap formation.

## ACKNOWLEDGMENTS

The authors would like to thank Dr. V. V. Kabanov. Y.T. acknowledges the support of the JSPS KAKENHI (JP19H05826, 19H02621).

- 
- [1] T. Timusk and B. Statt, The pseudogap in high-temperature superconductors: an experimental survey, *Rep. Prog. Phys.* **62**, 61 (1999).
- [2] K. M. Lang, V. Madhavan, J. E. Hoffman, E. W. Hudson, H. Eisaki, S. Uchida, and J. C. Davis, Imaging the granular structure of high- $T_c$  superconductivity in underdoped  $\text{Bi}_2\text{Sr}_2\text{CaCu}_2\text{O}_{8+\delta}$ , *Nature (London)* **415**, 412 (2002).
- [3] C. Howald, H. Eisaki, N. Kaneko, M. Greven, and A. Kapitulnik, Periodic density-of-states modulations in superconducting  $\text{Bi}_2\text{Sr}_2\text{CaCu}_2\text{O}_{8+\delta}$ , *Phys. Rev. B* **67**, 014533 (2003).
- [4] M. Vershinin, S. Misra, S. Ono, Y. Abe, Y. Ando, and A. Yazdani, Local ordering in the pseudogap state of the high- $T_c$  superconductor  $\text{Bi}_2\text{Sr}_2\text{CaCu}_2\text{O}_{8+\delta}$ , *Science* **303**, 1995 (2004).
- [5] T. Hanaguri, C. Lupien, Y. Kohsaka, D.-H. Lee, M. Azuma, M. Takano, H. Takagi, and J. Davis, A ‘checkerboard’ felectronic crystal state in lightly hole-doped  $\text{Ca}_{2-x}\text{Na}_x\text{CuO}_2\text{Cl}_2$ , *Nature (London)* **430**, 1001 (2004).
- [6] Y. Kohsaka, C. Taylor, K. Fujita, A. Schmidt, C. Lupien, T. Hanaguri, M. Azuma, M. Takano, H. Eisaki, H. Takagi, S. Uchida, and J. C. Davis, An intrinsic bond-centered electronic glass with unidirectional domains in underdoped cuprates, *Science* **315**, 1380 (2007).
- [7] T. Kurosawa, T. Yoneyama, Y. Takano, M. Hagiwara, R. Inoue, N. Hagiwara, K. Kurusu, K. Takeyama, N. Momono, M. Oda, and M. Ido, Large pseudogap and nodal superconducting gap in  $\text{Bi}_2\text{Sr}_{2-x}\text{La}_x\text{CuO}_{6+\delta}$  and  $\text{Bi}_2\text{Sr}_2\text{CaCu}_2\text{O}_{8+\delta}$ : Scanning tunneling microscopy and spectroscopy, *Phys. Rev. B* **81**, 094519 (2010).
- [8] D. H. Torchinsky, F. Mahmood, A. T. Bollinger, I. Bozovic, and N. Gedik, Fluctuating charge-density waves in a cuprate superconductor, *Nat. Mater.* **12**, 387 (2013).
- [9] S. A. Kivelson, E. Fradkin, and V. J. Emery, Electronic liquid-crystal phases of a doped mott insulator, *Nature (London)* **393**, 550 (1998).
- [10] G. Seibold and J. Lorenzana, Magnetic Fluctuations of Stripes in the High Temperature Cuprate Superconductors, *Phys. Rev. Lett.* **94**, 107006 (2005).
- [11] D. Fausti, R. I. Tobey, N. Dean, S. Kaiser, A. Dienst, M. C. Hoffmann, S. Pyon, T. Takayama, H. Takagi, and A. Cavalleri, Light-induced superconductivity in a stripe-ordered cuprate, *Science* **331**, 189 (2011).
- [12] T. Mertelj, V. V. Kabanov, and D. Mihailovic, Charged Particles on a Two-Dimensional Lattice Subject to Anisotropic Jahn-Teller Interactions, *Phys. Rev. Lett.* **94**, 147003 (2005).
- [13] T. Mertelj, V. V. Kabanov, J. M. Mena, and D. Mihailovic, Self-organization of charged particles on a two-dimensional lattice subject to anisotropic jahn-teller-type interaction and three-dimensional coulomb repulsion, *Phys. Rev. B* **76**, 054523 (2007).
- [14] H. Murayama, Y. Sato, R. Kurihara, S. Kasahara, Y. Mizukami, Y. Kasahara, H. Uchiyama, A. Yamamoto, E.-G. Moon,

- J. Cai *et al.*, Diagonal nematicity in the pseudogap phase of  $\text{HgBa}_2\text{CuO}_{4+\delta}$ , *Nat. Commun.* **10**, 3282 (2019).
- [15] K. Ishida, S. Hosoi, Y. Teramoto, T. Usui, Y. Mizukami, K. Itaka, Y. Matsuda, T. Watanabe, and T. Shibauchi, Divergent nematic susceptibility near the pseudogap critical point in a cuprate superconductor, *J. Phys. Soc. Jpn.* **89**, 064707 (2020).
- [16] M. Norman, H. Ding, M. Randeria, J. Campuzano, T. Yokoya, T. Takeuchi, T. Takahashi, T. Mochiku, K. Kadowaki, P. Guptasarma *et al.*, Destruction of the fermi surface in underdoped high- $T_c$  superconductors, *Nature (London)* **392**, 157 (1998).
- [17] K. Tanaka, W. Lee, D. Lu, A. Fujimori, T. Fujii, I. Terasaki, D. Scalapino, T. Devereaux, Z. Hussain, Z.-X. Shen *et al.*, Distinct fermi-momentum-dependent energy gaps in deeply underdoped  $\text{Bi2212}$ , *Science* **314**, 1910 (2006).
- [18] T. Kondo, T. Takeuchi, A. Kaminski, S. Tsuda, and S. Shin, Evidence for Two Energy Scales in the Superconducting State of Optimally Doped  $(\text{Bi, Pb})_2(\text{Sr, La})_2\text{CuO}_{6+\delta}$ , *Phys. Rev. Lett.* **98**, 267004 (2007).
- [19] T. Yoshida, M. Hashimoto, S. Ideta, A. Fujimori, K. Tanaka, N. Mannella, Z. Hussain, Z.-X. Shen, M. Kubota, K. Ono, S. Komiyama, Y. Ando, H. Eisaki, and S. Uchida, Universal Versus Material-Dependent Two-Gap Behaviors of the High- $T_c$  Cuprate Superconductors: Angle-Resolved Photoemission Study of  $\text{La}_{2-x}\text{Sr}_x\text{CuO}_4$ , *Phys. Rev. Lett.* **103**, 037004 (2009).
- [20] M. Oda, R. M. Dipasupil, N. Momono, and M. Ido, Hyperbolic dependence of  $2\delta_0$  vs.  $T_c$  ratio on hole-doping level in high- $T_c$  cuprates: Energy scale in determining  $T_c$ , *J. Phys. Soc. Jpn.* **69**, 983 (2000).
- [21] R. Nemeschek, M. Opel, C. Hoffmann, P. F. Müller, R. Hackl, H. Berger, L. Forró, A. Erb, and E. Walker, Pseudogap and Superconducting Gap in the Electronic Raman Spectra of Underdoped Cuprates, *Phys. Rev. Lett.* **78**, 4837 (1997).
- [22] H. Eisaki, N. Kaneko, D. L. Feng, A. Damascelli, P. K. Mang, K. M. Shen, Z.-X. Shen, and M. Greven, Effect of chemical inhomogeneity in bismuth-based copper oxide superconductors, *Phys. Rev. B* **69**, 064512 (2004).
- [23] A. Mumtaz, Y. Yamaguchi, K. Oka, and G. Rajaram, Effect of bi-sr replacement and oxygen doping on vortex-matter phase transitions in  $\text{Bi}_{2+x}\text{Sr}_{2-x}\text{CaCu}_2\text{O}_{8+\delta}$ , *Physica C: Superconductivity* **302**, 331 (1998).
- [24] Y. Okada, T. Takeuchi, A. Shimoyamada, S. Shin, and H. Ikuta, The influence of out-of-plane disorder on the formation of pseudogap and fermi arc in  $\text{Bi}_2\text{Sr}_{2-x}\text{R}_x\text{CuO}_y$  ( $r = \text{La}$  and  $\text{Eu}$ ), *J. Phys. Chem. Solids* **69**, 2989 (2008).
- [25] Y. Okada, T. Kawaguchi, M. Ohkawa, K. Ishizaka, T. Takeuchi, S. Shin, and H. Ikuta, Three energy scales characterizing the competing pseudogap state, the incoherent, and the coherent superconducting state in high- $T_c$  cuprates, *Phys. Rev. B* **83**, 104502 (2011).
- [26] T. Kurosawa, K. Takeyama, S. Baar, Y. Shibata, M. Kataoka, S. Mizuta, H. Yoshida, N. Momono, M. Oda, and M. Ido, Out-of-plane disorder effects on the energy gaps and electronic charge order in  $\text{Bi}_2\text{Sr}_{1.7}\text{R}_{0.3}\text{CuO}_{6+\delta}$  ( $r = \text{La}$  and  $\text{Eu}$ ), *J. Phys. Soc. Jpn.* **85**, 044709 (2016).
- [27] Y. H. Liu, K. Takeyama, T. Kurosawa, N. Momono, M. Oda, and M. Ido,  $4 \times 4$  a electronic charge order enhanced in the inhomogeneous pseudogap state of  $\text{Bi}_2\text{Sr}_2\text{CaCu}_2\text{O}_{8+\delta}$ , *Phys. Rev. B* **75**, 212507 (2007).
- [28] E. H. da Silva Neto, P. Aynajian, A. Frano, R. Comin, E. Schierle, E. Weschke, A. Gyenis, J. Wen, J. Schneeloch, Z. Xu *et al.*, Ubiquitous interplay between charge ordering and high-temperature superconductivity in cuprates, *Science* **343**, 393 (2014).
- [29] J. Demsar, B. Podobnik, V. V. Kabanov, T. Wolf, and D. Mihailovic, Superconducting Gap  $\delta_c$ , the Pseudogap  $\delta_p$ , and Pair Fluctuations Above  $T_c$  in Overdoped  $\text{Y}_{1-x}\text{Ca}_x\text{Ba}_2\text{Cu}_3\text{O}_{7-\delta}$  from Femtosecond Time-Domain Spectroscopy, *Phys. Rev. Lett.* **82**, 4918 (1999).
- [30] R. A. Kaindl, M. A. Carnahan, D. S. Chemla, S. Oh, and J. N. Eckstein, Dynamics of cooper pair formation in  $\text{Bi}_2\text{Sr}_2\text{CaCu}_2\text{O}_{8+\delta}$ , *Phys. Rev. B* **72**, 060510(R) (2005).
- [31] C. W. Luo, C. C. Hsieh, Y.-J. Chen, P. T. Shih, M. H. Chen, K. H. Wu, J. Y. Juang, J.-Y. Lin, T. M. Uen, and Y. S. Gou, Spatial dichotomy of quasiparticle dynamics in underdoped thin-film  $\text{YBa}_2\text{Cu}_3\text{O}_{7-\delta}$  superconductors, *Phys. Rev. B* **74**, 184525 (2006).
- [32] L. Perfetti, P. A. Loukakos, M. Lisowski, U. Bovensiepen, H. Eisaki, and M. Wolf, Ultrafast Electron Relaxation in Superconducting  $\text{Bi}_2\text{Sr}_2\text{CaCu}_2\text{O}_{8+\delta}$  by Time-Resolved Photoelectron Spectroscopy, *Phys. Rev. Lett.* **99**, 197001 (2007).
- [33] Y. H. Liu, Y. Toda, K. Shimatake, N. Momono, M. Oda, and M. Ido, Direct Observation of the Coexistence of the Pseudogap and Superconducting Quasiparticles in  $\text{Bi}_2\text{Sr}_2\text{CaCu}_2\text{O}_{8+y}$  by Time-Resolved Optical Spectroscopy, *Phys. Rev. Lett.* **101**, 137003 (2008).
- [34] C. Giannetti, F. Cilento, S. Dal Conte, G. Coslovich, G. Ferrini, H. Molegraaf, M. Raichle, R. Liang, H. Eisaki, M. Greven, A. Damascelli, D. van der Marel, and F. Parmigiani, Revealing the high-energy electronic excitations underlying the onset of high-temperature superconductivity in cuprates, *Nat. Commun.* **2**, 353 (2011).
- [35] J. Graf, C. Jozwiak, C. L. Smallwood, H. Eisaki, R. A. Kaindl, D. H. Lee, and A. Lanzara, Nodal quasiparticle meltdown in ultrahigh-resolution pump-probe angle-resolved photoemission, *Nat. Phys.* **7**, 805 (2011).
- [36] Y. Toda, T. Mertelj, P. Kusar, T. Kurosawa, M. Oda, M. Ido, and D. Mihailovic, Quasiparticle relaxation dynamics in underdoped  $\text{Bi}_2\text{Sr}_2\text{CaCu}_2\text{O}_{8+\delta}$  by two-color pump-probe spectroscopy, *Phys. Rev. B* **84**, 174516 (2011).
- [37] G. Coslovich, C. Giannetti, F. Cilento, S. Dal Conte, T. Abebaw, D. Bossini, G. Ferrini, H. Eisaki, M. Greven, A. Damascelli, and F. Parmigiani, Competition between the Pseudogap and Superconducting States of  $\text{Bi}_2\text{Sr}_2\text{Ca}_{0.92}\text{Y}_{0.08}\text{Cu}_2\text{O}_{8+\delta}$  Single Crystals Revealed by Ultrafast Broadband Optical Reflectivity, *Phys. Rev. Lett.* **110**, 107003 (2013).
- [38] Y. Toda, F. Kawanokami, T. Kurosawa, M. Oda, I. Madan, T. Mertelj, V. V. Kabanov, and D. Mihailovic, Rotational symmetry breaking in  $\text{Bi}_2\text{Sr}_2\text{CaCu}_2\text{O}_{8+\delta}$  probed by polarized femtosecond spectroscopy, *Phys. Rev. B* **90**, 094513 (2014).
- [39] I. Madan, T. Kurosawa, Y. Toda, M. Oda, T. Mertelj, and D. Mihailovic, Evidence for carrier localization in the pseudogap state of cuprate superconductors from coherent quench experiments, *Nat. Commun.* **6**, 6958 (2015).
- [40] I. Madan, V. V. Baranov, Y. Toda, M. Oda, T. Kurosawa, V. V. Kabanov, T. Mertelj, and D. Mihailovic, Dynamics of superconducting order parameter through ultrafast normal-to-superconducting phase transition in  $\text{Bi}_2\text{Sr}_2\text{CaCu}_2\text{O}_{8+\delta}$  from

- multipulse polarization-resolved transient optical reflectivity, *Phys. Rev. B* **96**, 184522 (2017).
- [41] D. C. Johnston, Magnetic Susceptibility Scaling in  $\text{La}_{2-x}\text{Sr}_x\text{CuO}_{4-y}$ , *Phys. Rev. Lett.* **62**, 957 (1989).
- [42] M. Oda, T. Ohguro, N. Yamada, and M. Ido, Magnetic susceptibility and superconductivity in  $(\text{La}_{1-x}\text{Sr}_x)_2\text{CuO}_4$ , *J. Phys. Soc. Jpn.* **58**, 1137 (1989).
- [43] T. Nakano, M. Oda, C. Manabe, N. Momono, Y. Miura, and M. Ido, Magnetic properties and electronic conduction of superconducting  $\text{La}_{2-x}\text{Sr}_x\text{CuO}_4$ , *Phys. Rev. B* **49**, 16000 (1994).
- [44] P. Kusar, V. V. Kabanov, S. Sugai, J. Demsar, T. Mertelj, and D. Mihailovic, Controlled Vaporization of the Superconducting Condensate in Cuprate Superconductors by Femtosecond Photoexcitation, *Phys. Rev. Lett.* **101**, 227001 (2008).
- [45] L. Stojchevska, P. Kusar, T. Mertelj, V. V. Kabanov, Y. Toda, X. Yao, and D. Mihailovic, Mechanisms of nonthermal destruction of the superconducting state and melting of the charge-density-wave state by femtosecond laser pulses, *Phys. Rev. B* **84**, 180507(R) (2011).
- [46] V. V. Kabanov, J. Demsar, B. Podobnik, and D. Mihailovic, Quasiparticle relaxation dynamics in superconductors with different gap structures: Theory and experiments on  $\text{YBa}_2\text{Cu}_3\text{O}_{7-\delta}$ , *Phys. Rev. B* **59**, 1497 (1999).
- [47] N. Gedik, P. Blake, R. C. Spitzer, J. Orenstein, R. Liang, D. A. Bonn, and W. N. Hardy, Single-quasiparticle stability and quasiparticle-pair decay in  $\text{YBa}_2\text{Cu}_3\text{O}_{6.5}$ , *Phys. Rev. B* **70**, 014504 (2004).
- [48] V. V. Kabanov, J. Demsar, and D. Mihailovic, Kinetics of a Superconductor Excited with a Femtosecond Optical Pulse, *Phys. Rev. Lett.* **95**, 147002 (2005).
- [49] I. Madan, P. Kusar, V. V. Baranov, M. Lu-Dac, V. V. Kabanov, T. Mertelj, and D. Mihailovic, Real-time measurement of the emergence of superconducting order in a high-temperature superconductor, *Phys. Rev. B* **93**, 224520 (2016).